A "twisted" visual field map in the primate cortex predicted by topographic continuity

Hsin-Hao Yu[1,2], Declan P. Rowley[1,2], Elizabeth Zavitz[1,2], Nicholas S.C. Price[1,2], Marcello G.P. Rosa[1,2*]

1- Department of Physiology and Biomedicine Discovery Institute – Neuroscience Program, Monash University, Clayton, 3800 Victoria, Australia
2- ARC Centre of Excellence for Integrative Brain Function, Monash University, Clayton, 3800 Victoria, Australia

* Corresponding author

Abstract

Adjacent neurons in sensory cortex have overlapping receptive fields within and across area boundaries. In early visual cortex this creates areas with mirror or non-mirror representations of the visual field, an arrangement which is theorized to minimize wiring cost. We demonstrate that a more complex map consisting of both types of representation exists in an extrastriate area, and show how this can emerge from a mechanism that maintains topographic continuity.

Keywords

- Dorsomedial area
- Extrastriate cortex
- Retinotopic organization
- Wire length minimization
- Marmoset
- Computational model
- Multielectrode arrays

Sensory cortices represent the world in a mosaic of topographically organized maps. In the visual cortex, neurons in adjacent columns have overlapping receptive fields, both within each area and across area boundaries. What are the benefits of this local mapping continuity, and how does it constrain the global topology of cortical maps? A prominent theory, which postulates that this continuity is effective in minimizing the wiring cost of the underlying circuits[1], can explain why retinotopic maps in early visual areas (e.g., V1, V2) are organized as alternating mirror and non-mirror representations of the visual field[2,3]. However, it is unclear to what extent this applies to higher-order regions, where areas do not follow the concentric ring geometry of V1/V2, and receptive fields are larger[3,4]. Indeed, reports of fractured and incomplete maps[4,5] suggest that continuity might be violated or relaxed in some situations. The lack of fine-scale quantitative studies of these apparent discontinuities, as well as the limited understanding of the principles that underlie the formation of maps in higher-order areas, have resulted in many controversies in brain mapping[5-8].

Here we focused on a "third-tier" region of the primate visual cortex, where the concentric arrangement of V1 and V2 gives way to a patchwork of smaller areas[3-6]. This transition introduces a new level of complexity into retinotopy, because unlike in V1 and V2, where the upper and the lower quadrants of the visual field are represented separately in ventral and dorsal cortex[2], some of the areas in this region contain representations of both the upper and the lower quadrants adjacent to the lower field representation of V2[3,6,8]. Specifically, we examined the retinotopy of the putative dorsomedial area (DM) of the New World marmoset monkey visual cortex, whose organization has been disputed for decades[6]. Based on histology, connectivity and single-unit electrophysiology, it has been proposed that this region is primarily occupied by a single area, which would have the unusual characteristics of an internal discontinuity in retinotopy (Fig 1a, red stars), as well as sectors of both mirror- and non-mirror representation of the visual field[8-10] (Fig 1a). Others, however, see this putative area DM as the union of multiple areas, each forming a more conventional representation[7,11].

To clarify its organization**,** we quantified receptive field locations and response properties of neurons in the region surrounding the rostral border of dorsal V2 (lower quadrant representation, V2-), using 10x10 multielectrode arrays with 400 μm electrode spacing (Fig. 1; Supplementary Figs. S1-5). Our data indicated that immediately rostral to V2- is a representation of the contralateral visual field covering at least to 20° in eccentricity (Fig. 1b,c). The upper quadrant (referred to here as DM+) is represented laterally, and the lower quadrant (DM-) medially. Both DM+ and DM- border V2- along a continuous representation of the horizontal meridian. This organization is consistent with an earlier model of the retinotopy of area DM[9,10] (Fig. 1a), but not with the interpretation which postulates the existence of an additional thin stripe of "area V3" (representing the lower visual field) sandwiched between V2- and DM[7,11].

Earlier work[9,10] has suggested that the transition between DM+ and DM- includes a "map discontinuity" (arrow in Fig. 1a) - a sudden "jump" of receptive field centers between closely spaced recording sites, which violated topographic continuity[3]. However, receptive fields mapping in those studies was qualitative, and the sampling was uneven across the cortical surface, demanding a more rigorous approach[7]. Using electrode arrays to sample the cortical surface uniformly, and mapping receptive fields with a quantitative procedure, we confirmed that the transition between DM+ and DM- is retinotopically unusual: the representations of central vision (<5° eccentricity) in DM+ and DM- (Fig. 2a) appeared disjoined, and crossing the DM+/DM- boundary resulted in a distinctive "S"-shape trajectory of receptive field centers across the horizontal meridian (Fig. 2c). However, the receptive fields of adjacent recording sites were still overlapping, indicating that the boundary is more accurately characterized as a thin strip of cortex with an eccentricity gradient that rapidly reverses polarity (Fig. 2b), rather than a true map discontinuity.

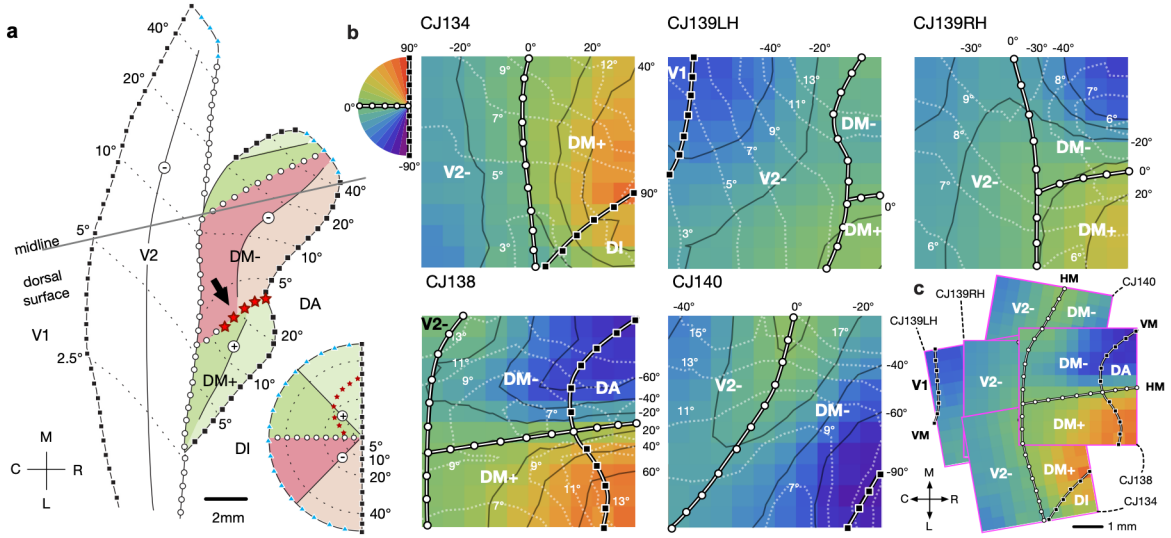

Fig 1: Retinotopy of the marmoset dorsomedial cortex (**a**) A schematic summary of one of the competing models of organization of dorsomedial cortex in the marmoset[9]. The inset at the bottom right illustrates the color scheme used to illustrate different segments of the visual hemifield in the proposed area DM. The arrow indicates the location of the putative "map discontinuity". (**b**) The retinotopy of 5 hemispheres from 4 animals (identifiers of the cases are prefixed by "CJ"), estimated from receptive fields mapped using 10x10 electrode arrays. The colors represent the polar angles. Polar angles are indicated by solid black contours and numbers in black. Eccentricities are indicated by dashed white lines and numbers in white. Inset: The color scale for representing the polar angle in **b** and **c**. The horizontal meridian (polar angle=0°) is indicated by thick lines overlaid with circles. The vertical meridian (polar angle ±90°) is indicated by thick lines and squares. (**c**) Composite summary of the spatial relationships shown in **b**. Abbreviations: V1: primary visual area; V2-: dorsal portion of second visual area; DM+/-: upper/lower field representation of the dorsomedial area; DA: dorsoanterior area; DI: dorsointermediate area; M: medial; L: lateral; C: caudal; R: rostral.

"Field sign" is a technique for detecting regions of coherent retinotopy, and is commonly used to identify visual areas[3,12,13]. Sites within DM+ and DM- have opposite field signs (Fig. 2d,e), which is normally taken as evidence that they are two different areas[3,13]. However, caution should be taken in the interpretation of field sign, because in this situation, the DM+ and DM- maps are not mirror-

images of each other. Given the similarity between DM+ and DM- in terms of connectivity[10,14], cortical magnification factor, receptive field size, and response characteristics (Supplementary Fig. S6), we sought to explain the unusual retinotopy as a consequence of topographic continuity under constraints imposed by the adjacency with V2-.

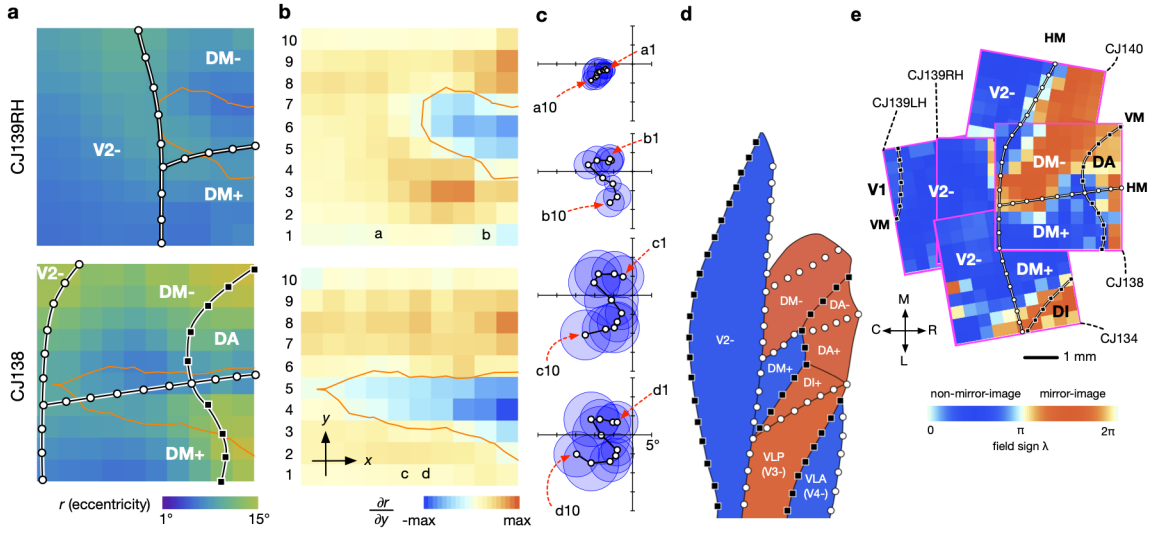

Fig 2: Local features of the DM map (**a**) Eccentricity maps of two selected cases. The cortex enclosed by the orange contours indicates a region where the gradient of the eccentricity rapidly reversed polarity. (**b**) This region can be visualized by plotting the partial gradient of eccentricity with respect to the spatial dimension of the rows (the y-axis) of the electrode arrays. The region in blue (enclosed by the orange contour) corresponds to sites where the eccentricity of the receptive field rapidly decreased in the lateral-to-medial direction. (**c**) Representative sequences of receptive fields associated with channels in columns of the electrode arrays. The association between the receptive fields and the channels are identified by letters (columns) and numbers (rows). The progressions of receptive fields followed a distinctive "S"-shape trajectory. (**d**) A summary of the field signs for areas in the dorsomedial region of the marmoset visual cortex. The field signs for area DM, DI, VLP (ventrolateral posterior area, or V3) and VLA (ventrolateral anterior area, or V4) were inferred from published maps[9,10]. **(e)** Field sign maps estimated for the 5 cases.

We simulated the formation of the retinotopic map adjacent to the rostral border of dorsal V2, by extending a general framework for modelling the development of cortical topographic maps (elastic net[1,15]). In this model, "DM" neurons were distributed on a 2D grid representing the surface of the cortex, and their receptive field centers were optimized to cover a set of points distributed regularly in the visual field. The optimization was constrained by two terms in the cost function, where the β_1 parameter governs map smoothness (increasing β_1 prioritizes matching receptive field locations of neighboring DM neurons), and the β_2 parameter governs congruence (increasing β_2 prioritizes matching the receptive field locations between V2- and DM neurons at the area boundary).

As the balance between within-area smoothness and between-area congruence was manipulated, three types of maps emerged (Fig. 3i). At moderate levels of β_1 and β_2, the developed retinotopy was similar to the map of V1 and V2 (Fig. 3e); the eccentricity and polar angle maps were continuous, and the entire map had the same field sign (Fig. 3f). As the smoothness constraint ($\beta 1$) decreased, however, the map divided into two regions with opposite field signs (Fig. 3b). The representations of

the central upper and lower visual fields were disjointed (Fig. 3a), and crossing the map yielded an "S"-shaped trajectory (Fig. 3c), similar to our experimental data (Fig. 2c). This map can be considered a "twisted" version of the first map (compare Fig. 3d with 3h). The twist rotated the direction of the eccentricity gradient, which reversed the polarity of the field sign, without making DM+ and DM- mirror images of each other. Finally, at high values of β_1 and β_2, another type of map with two regions with opposing field signs developed. This is a more complex map (the representation of the fovea in the lower field is displaced from the rest of the lower field representation) that does not seem to correspond to the known organization of any visual area yet described.

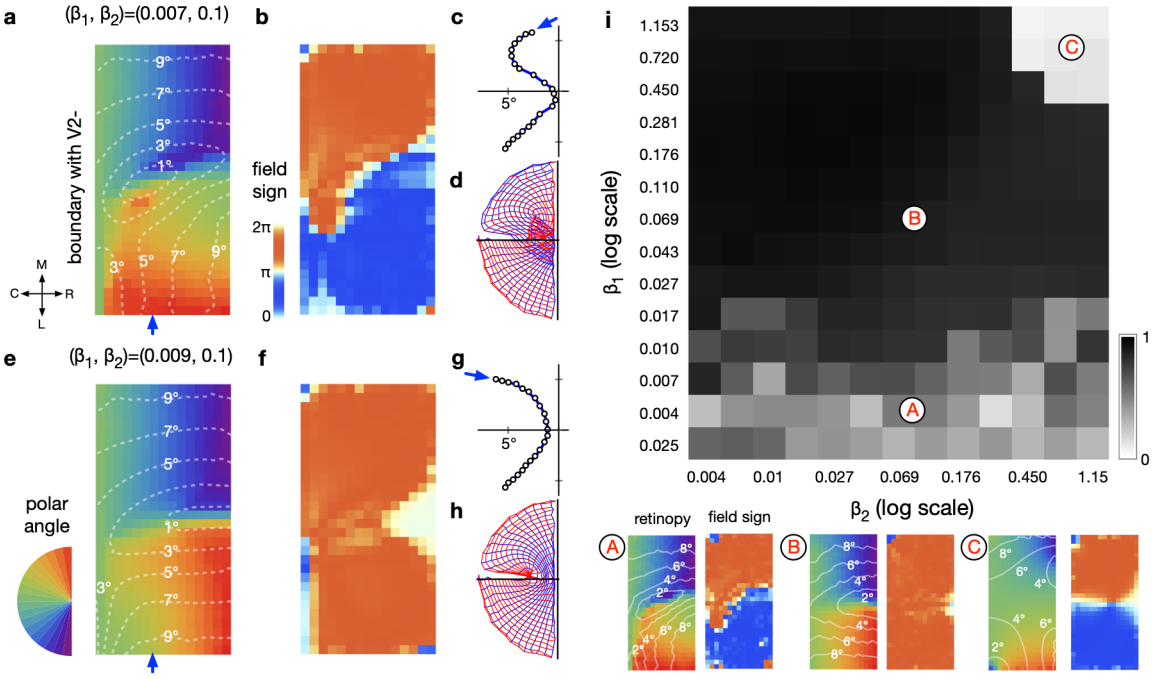

Fig. 3|Simulations of DM map formation. The model produced three types of maps depending on the combinations of β1 and β2. **a-d** illustrates a setting where a map similar to the map shown in Figure 2 emerged. (**a**) Retinotopic coordinates, where colors represent the polar angle, and the dashed white contours represent eccentricity. (**b**) field signs. (**c**) Moving an electrode in the direction indicated by the blue arrow in **a** yielded receptive fields that progressed in a "S"-shaped trajectory, similar to what was shown in Figure 2c. (**d**) The grid of the cortical map (blue: columns; red: rows), is mapped onto the corresponding receptive field locations on the visual field. (**e-h**) At a slightly higher setting of β1, a simpler map developed. (**i**) The dependency between the two parameters and the field sign of the resulting map. The grey scale represents the averaged field sign, scaled to -1 to 1, across the map and across 8 repeats of randomly initialized simulations. It measures the complexity of the maps: values close to 0 indicate maps with balanced regions of opposing field signs, whereas values close to 1 indicate maps dominated by the mirror image field sign. Regions indicated by A, B, and C correspond to the three types of maps illustrated below.

In summary, we used bias-free receptive field mapping to clarify the organization of a controversial region of the marmoset visual cortex, and demonstrated that the unusual retinotopy of this region can arise naturally from the same mechanism hypothesized to promote the configuration of early areas such as V1 and V2. Due to the similarity between DM+ and DM- in terms of histology, connectivity, receptive field size, cortical magnification factor, and response properties (Supplementary Fig. S6),

the modeling result further supports the notion that DM- and DM+ are parts of the same area (area DM), located immediately rostral to dorsal V2[2,8].

This organization is not unique to the marmoset. Sereno *et al.*[3] reported a similar organization in the owl monkey visual cortex, but identified the region that we designated DM+ as a separate area DI+, due to its field sign being different from the more medial region (approximately corresponding to our DM-). This proposal prioritized the unity of field sign within areas, but it resulted in an area DI+ that represents only the upper visual field. We argue that whereas in many cases the areal boundaries can be readily identified by the reversals of field sign, regions of opposing field signs can also arise naturally within a single area based on a similar developmental mechanism[16,17]. The interpretation of field sign therefore must take the context of the global map across areas into account. The organization of DM might be applicable to Old World monkeys as well, as a recent high-resolution fMRI mapping study of the macaque visual cortex demonstrated an organization that shares striking similarity with that of the marmoset dorsomedial cortex[18]. In addition, electrophysiological mapping[19] and anatomical studies[20] have suggested that a DM homologue, adjacent to V2, also exists in macaques.

Two types of discontinuity in topographic maps can be distinguished[5,21]: *field discontinuity* (i.e., overlapping regions on the visual fields mapped to non-overlapping regions on the cortical surface) and *map discontinuity* (i.e., overlapping regions on the cortical surface mapped to non-overlapping regions on the visual field). While field discontinuities are well-documented (e.g., the rostral boundary of V2), the existence of map discontinuities has been controversial. We showed that the topographic transition at the DM+/DM- boundary is more appropriately characterized as a thin strip of cortex with rapidly changing eccentricity gradient, rather than true a map discontinuity. Some of the uncertainties and controversies in the mapping of extrastriate areas might be due to this novel type of areal boundary, because the reversal of eccentricity gradient might be undetected by the typical resolution of fMRI.

We showed that different types of retinotopic maps can emerge depending on the balance between within-area continuity and betw(een-area congruency. While the developmental factors that determine the strength of these two constraints remain unknown, our simulation indicates that the DM map was formed in a regime where between-area congruency was prioritized over within-area continuity. This situation may emerge from a scenario where topographic maps in different areas develop asynchronously, with a pre-existing map in an early-maturing area constraining the possible receptive field locations at the border with a late-maturing area[16,17]. Congruency allows multiple areas to form large-scale supra-areal clusters, which have been proposed as the fundamental building block of

cortical organization[22]. Studying the consequence of continuity constrains, in the context of the geometrical relationship between areas, is critical for the understanding of these large-scale structures.

Acknowledgements

The authors thank Dr. Geoffrey Goodhill for comments on an earlier version of this manuscript, Katrina Worthy for the expert help in setting up experiments and histology, and Janssen-Cilag for providing sufentanil citrate. Funded by project grants from the Australian Research Council (ARC, DP170104600) and National Health and Medical Research Council (NHMRC, 1128755), and by the ARC Centre of Excellence for Integrative Brain Function (CE140100007).

References

1. Durbin, R. & Mitchison, G. A dimension reduction framework for understanding cortical maps. *Nature* **343**, 644-647 (1990).

2. Allman, J.M. & Kaas, J.H. The organization of the second visual area (V II) in the owl monkey: a second order transformation of the visual hemifield. *Brain Res.* **76**, 247-265 (1974).

3. Sereno, M.I., McDonald, C.T. & Allman, J.M. Retinotopic organization of extrastriate cortex in the owl monkey—dorsal and lateral areas. *Vis. Neurosci.* **32**, e21 (2015).

4. Allman, J.M. & Kaas, J.H. The dorsomedial cortical visual area: a third tier area in the occipital lobe of the owl monkey (*Aotus trivirgatus*). *Brain Res.* **100**, 473-487 (1975).

5. Rosa, M.G.P. & Tweedale, R. Maps of the visual field in the cerebral cortex of primates: functional organization and significance. In: *The Primate Visual System* (Kaas, J.H. and Collins, C.E., eds.), pp. 261-288. CRC Press, Boca Raton, 2004.

6. Angelucci, A. & Rosa, M.G.P. Resolving the organization of the third tier visual cortex in primates: a hypothesis-based approach. *Vis. Neurosci.* **32**, e010 (2015).

7. Lyon, D.C. & Connolly, J.D. The case for primate V3. *Proc. R. Soc. Lond. B. Biol. Sci.* **279**, 625-33 (2012).

8. Rosa, M.G.P., Angelucci, A., Jeffs, J. & Pettigrew, J.D. The case for a dorsomedial area in the primate 'third-tier' visual cortex. *Proc. R. Soc. Lond. B. Biol. Sci.* **280**, 20121372 (2013).

9. Rosa, M.G.P. & Schmid, L.M. Visual areas in the dorsal and medial extrastriate cortices of the marmoset. *J. Comp. Neurol.* **359**, 272-299 (1995).

10. Rosa, M.G.P. et al. Connections of the dorsomedial visual area: pathways for early integration of dorsal and ventral streams in extrastriate cortex. *J. Neurosci.* **29**, 4548-4563 (2009).

11. Lyon, D.C. & Kaas, J.H. Connectional and architectonic evidence for dorsal and ventral V3, and dorsomedial area in marmoset monkeys. *J. Neurosci.* **21**, 249-261 (2001).

12. Sereno, M.I., McDonald, C.T. & Allman, J.M. Analysis of retinotopic maps in extrastriate cortex. *Cereb. Cortex* **4**, 601-620 (1994).

13. Sereno, M.I., Dale, A.M., Reppas, J.B., Kwong, K.K., Belliveau, J.W., Brady, T.J., Rosen, B.R. & Tootell, R.B. 1995. Borders of multiple visual areas in humans revealed by functional magnetic resonance imaging. *Science* **268**, 889-893 (1995).

14. Jeffs, J., Rederer, F., Ichida, J.M. & Angelucci, A. High-resolution mapping of anatomical connections in marmoset extrastriate cortex reveals a complete representation of the visual field bordering dorsal V2. *Cereb. Cortex* **23**, 1126-1147 (2013).

15. Goodhill, G.J. & Willshaw, D.J. Application of the elastic net algorithm to the formation of ocular dominance stripes. *Network* **1**, 41-59 (1990).

16. Rosa, M.G.P. Visual maps in the adult primate cerebral cortex: some implications for brain development and evolution. *Braz. J. Med. Biol. Res.* **35**, 1485-1498 (2002).

17. Rosa, M.G.P. & Tweedale, R. Brain maps, great and small: lessons from comparative studies of primate visual cortical organization. *Philos. Trans. R. Soc. Lond. B. Biol. Sci.* **360**, 665-691 (2005).

18. Zhu,Q. & Vanduful, W. Submillimeter fMRI reveals a layout of dorsal visual cortex in macaques, remarkably similar to New World monkeys. *Proc. Natl. Acad. Sci. USA* **116**, 2306–2311 (2019).

19. Hadjidimitrakis, K., Bakola, S., Chaplin, T.A., Yu, H.H., Alanazi, O., Chan, J.M., Worthy, K.H. & Rosa MGP. 2019. Topographic organization of the "third tier" dorsomedial visual cortex in the macaque. *J. Neurosci.* doi: 10.1523/JNEUROSCI.0085-19.2019. [Epub ahead of print]

20. Beck, P.D., & Kaas, J.H. Cortical connections of the dorsomedial visual area in old world macaque monkeys. *J. Comp. Neurol.* 406, 487-502 (1998).

21. Van Essen, D. C., Maunsell, J. H. R. & Bixby, J. L. The middle temporal visual area in the macaque: Myeloarchitecture, connections, functional properties and topographic organization. *J. Comp Neurol.* **199**, 293-326 (1981).

22. Arcaro, M.J. & Kastner, S. Topographic organization of areas V3 and V4 and its relation to supra-areal organization of the primate visual system. *Vis. Neurosci*. **32**, e14 (2015).

Methods

Preparation. Experiments were conducted in accordance with the Australian Code of Practice for the Care and Use of Animals for Scientific Purposes. All procedures were approved by the Monash University Animal Ethics Experimentation Committee. In four marmoset monkeys (*Callithrix jacchus*) surgical anaesthesia was induced by intramuscular injection of alfaxalone (Alfaxan, 8mg/kg). Under anaesthesia, the animal was injected with an antibiotic (Norocillin, 25mg/kg) and dexamethasone (Dexason, 0.3mg/kg). A tracheotomy was performed, and the femoral artery was cannulated. The animal was positioned in a stereotaxic frame, and a craniotomy and durotomy were performed over DM[23]. For the duration of the recording session, the animal was maintained on infusion of sufentanil citrate (Sufenta Forte, 250µg/5ml), pancuronium bromide (Pancronium, 4mg/2ml), dexamethasone (Dexapent, 5mg/ml), xylazine (Xylazil-20, 20mg/ml) and salts and nutrients (0.18% NaCl/4% glucose solution, Synthamine-13 and Hartmann's solution), and ventilated with a nitrous oxide and oxygen mixture (7:3). The animal's body temperature was kept at a steady 38 degrees, measured by rectal thermometer. The eye contralateral to the craniotomy was held open, and atropine (Atropt, 1%), phenylephrine, and carmellose sodium (Celluvisc) eye drops applied, before a contact lens was inserted to focus the eye at a viewing distance of 20-40cm. The ipsilateral eye was protected with carmellose sodium, closed, and occluded.

Electrophysiology. 10x10 "Utah" arrays (Blackrock Microsystems, Salt Lake City, USA) with 96 active channels, were implanted in area DM using a pneumatic insertion tool. The position of DM was located using stereotaxic coordinates *in vivo* and verified with flatmount histology *post mortem* (Supplementary Figure 7). Electrodes were 1.5mm long, and spaced at 100µm intervals. The raw voltage signal was recorded at 30kHz using a Cerebus system (Blackrock Microsystems, Salt Lake City, USA) and high-pass filtered at 750Hz. Spikes were detected using automatic thresholding of the local signal. After recording, manual spike sorting was performed offline using Plexon Offline Sorter (Plexon Inc., Dallas, USA).

Visual stimulation.

The positions of several receptive fields in space were hand-mapped on a tangent screen, and a VIEWPixx 3D (VPixx Technologies, Saint-Bruno, Canada) positioned at a viewing distance of 350-450 mm with the receptive fields in and around the center of the monitor. The stimuli were presented at a 120Hz refresh rate using The Psychophysics Toolbox in MATLAB[24-26]. Receptive fields were mapped at 1° resolution with both "on" (white) and "off" (black) squares flashed on a grey background. Squares appeared for 100 ms with a 50-to-100 ms (different in different cases) inter-stimulus interval.

Retinotopy. To quantify the geometry of the receptive fields, the spike counts elicited by each location of the flashing square stimulus were smoothed with a 5x5 Gaussian kernel. A Gaussian function was fitted to the smoothed map (EQ. 1), where (μ_x, μ_y) is the center of the receptive field. The boundary of the receptive field (and therefore its size) was determined by the contour at 15% of the peak response.

$$r = c + e^{\frac{1}{2}\left(-\frac{(x-\mu_x)^2}{\sigma} - \frac{(y-\mu_y)^2}{\sigma}\right)} \quad \text{EQ. 1}$$

The center of gaze was inferred from the retinotopy, given that at the boundary of visual areas, the progression of the receptive fields reverses its direction at the horizontal or the vertical meridian. For CJ134, CJ138, CJ140, the locations of the blind spot could be identified in the receptive field maps (Figs. S1, S4, S5). Because the representation of the blind spot on the visual field is approximately 15° away from the fovea on the horizontal meridian[27], this imposed a strong constraint on the location of the center of gaze.

Field sign. Field sign (λ) is defined as the clockwise angle between the eccentricity gradient and the polar angle gradient[12]. For calculating the gradients, the coordinates of the receptive field centers were smoothed by moving window averaging. The field signs calculated for individual channels were then smoothed by moving window averaging. For visualization, the calculated field sign was compressed by a sigmoid function[11] and then displayed with a color scale such that non-mirror image maps ($0<\lambda<\pi$) appear bluish and mirror-image maps ($\pi<\lambda<2\pi$) appear reddish.

Simulation. A modified version of the elastic net algorithm[15] was used to solve the proximate minimal path length problem[1]. The model consisted of neurons with point receptive fields (y_j) initialized to random locations on the contralateral visual hemifield within 10° of eccentricity. These receptive fields are arranged topologically in a 30x15 grid modeling area DM, and they were updated iteratively using gradient descent to minimize the energy function (EQ. 2):

$$E = -k\sum_i log\sum_j \Phi\left(x_i, y_j, k\right) + \beta_1\sum_j\sum_{j'\in N(j)}\left\|y_{j'} - y_j\right\|^2 + \beta_2\sum_{j\in B}\sum_{j'\in N_{V2}(j)}\left\|z_{j'} - y_j\right\|^2 \quad \text{EQ. 2}$$

The first term is a "coverage term" that forces y_j to converge to 500 fixed points (x_i) distributed regularly on the visual hemifield up to 10° of eccentricity, with a density that dropped off with eccentricity (density $\propto$ eccentricity$^{-0.4}$). $\Phi(x_i, y_j, k) = exp(\frac{-\|x_i - y_j\|^2}{2k^2})$, where k is an annealing factor that was initialized to 30.0, and reduced by 0.5% for each iteration. The regular distribution of x_i was

implemented with the Vogel method. The coverage term is followed by two regularization terms to enforce topographic continuity, which were weighted by two parameters $\beta_1$and β_2. The first regularization term enforces the smoothness of the retinotopy, where $N(j)$ denotes sites on the 30x15 grid that neighbor site j. The second regularization term enforces congruency with the retinotopy of V2 at the caudal boundary of DM (denoted by B), where $N_{V2}(j)$ denotes sites in V2 which neighbor site j in DM. V2 receptive fields are located at $z_{j'}$, which are fixed points on the horizontal meridian. The range of eccentricity at the DM/V2 boundary was 2° to 10.0°. The model was implemented with Tensorflow and the source code is available at https://github.com/hsinhaoyu/DM_Retinotopy.

Cortical magnification factor. The reciprocal of the (linear) cortical magnification factor[28] $1/M$ was calculated as $\sqrt{1/M_a}$, where $1/M_a = |\det(J)|$, J being the Jacobian matrix of the mapping from the cortex surface to the visual field[29]. This measures the linear cortical magnification factor M from the areal cortical magnification factor M_a assuming that the mapping is isotropic. The calculation of J was based on the locations of the measured receptive field centers without smoothing. The estimated $1/M$ was then spatially smoothed.

Orientation tuning. We used drifting sinusoidal gratings to determine the preferred orientation for the units on the array. Spatial and temporal frequency were selected to best drive the largest number of units possible and ranged from 0.3 to 1 cycle/° and 2.5 to 4 Hz. Responses were measured for 24 directions, tiling 360° at 15° intervals to motion lasting 400 to 1000 ms. The preferred orientation was determined based on the resultant vector[30], and the bandwidth with the circular variance of the responses[31].

Histology. After the completion of data collection, the animal was given a lethal overdose of sodium pentobarbitone (100mg/kg). The array was removed and the animal transferred to a fume hood where it was perfused with buffered saline. The unfixed brain was immediately extracted, and the two hemispheres were separated and physically flat-mounted. Flat-mounting (Fig. S7) was performed by gently dissecting away the white matter of the cortex with dry cotton swabs, with the cortex supported on a piece of moist filter paper (pial surface down). Relaxation cuts were made in the fundus of the calcarine sulcus, and at the anterior end of the sylvian sulcus to allow the cortex to lie flat. The cortex was held in fixative between two large glass slides under a small weight overnight, and then was soaked in sucrose solution in increasing concentrations (10%, 20% and 30%). The flat-mounted hemisphere was then cut in a cryostat to a thickness of 40 µm. Alternate sections were stained for myelin and cytochrome oxidase.

References

23. Paxinos, G., Watson, C., Petrides, M., Rosa, M. & Tokuno, H. *The marmoset brain in stereotaxic coordinates*. (Elsevier Academic Press, 2012).

24. Brainard, D. H. & Vision, S. The psychophysics toolbox. *Spat. Vis.* **10**, 433–436 (1997).
25. Kleiner, M. et al. What's new in Psychtoolbox-3. *Perception* **36,** 1 (2007).
26. Pelli, D. G. The VideoToolbox software for visual psychophysics: transforming numbers into movies. *Spat. Vis*. **10**, 437–442 (1997).
27. Troilo, D., Rowland, H.C. & Judge, S.J. Visual optics and retinal cone topography in the common marmoset (*Callithrix jacchus*). *Vision Res.* 33, 1301-1310 (1993).
28. Daniel, P.M. & Whitteridge, D. The representation of the visual field on the cerebral cortex in monkeys. *J. Physiol.* **159**, 203-221 (1961).
29. Schwartz, E. Anatomical and physiological correlates of visual computation from striate to infero-temporal cortex. *IEEE Trans Syst Man Cybern B Cybern SMC* **14**, 257-271 (1984).
30. Ringach, D. L., Shapley, R. M. & Hawken, M. J. Orientation selectivity in macaque V1: diversity and laminar dependence. *J. Neurosci.* **22**, 5639–5651 (2002).
31. Berens, P. & Others. CircStat: a MATLAB toolbox for circular statistics. *J. Stat. Softw.* **31**, 1–21 (2009).

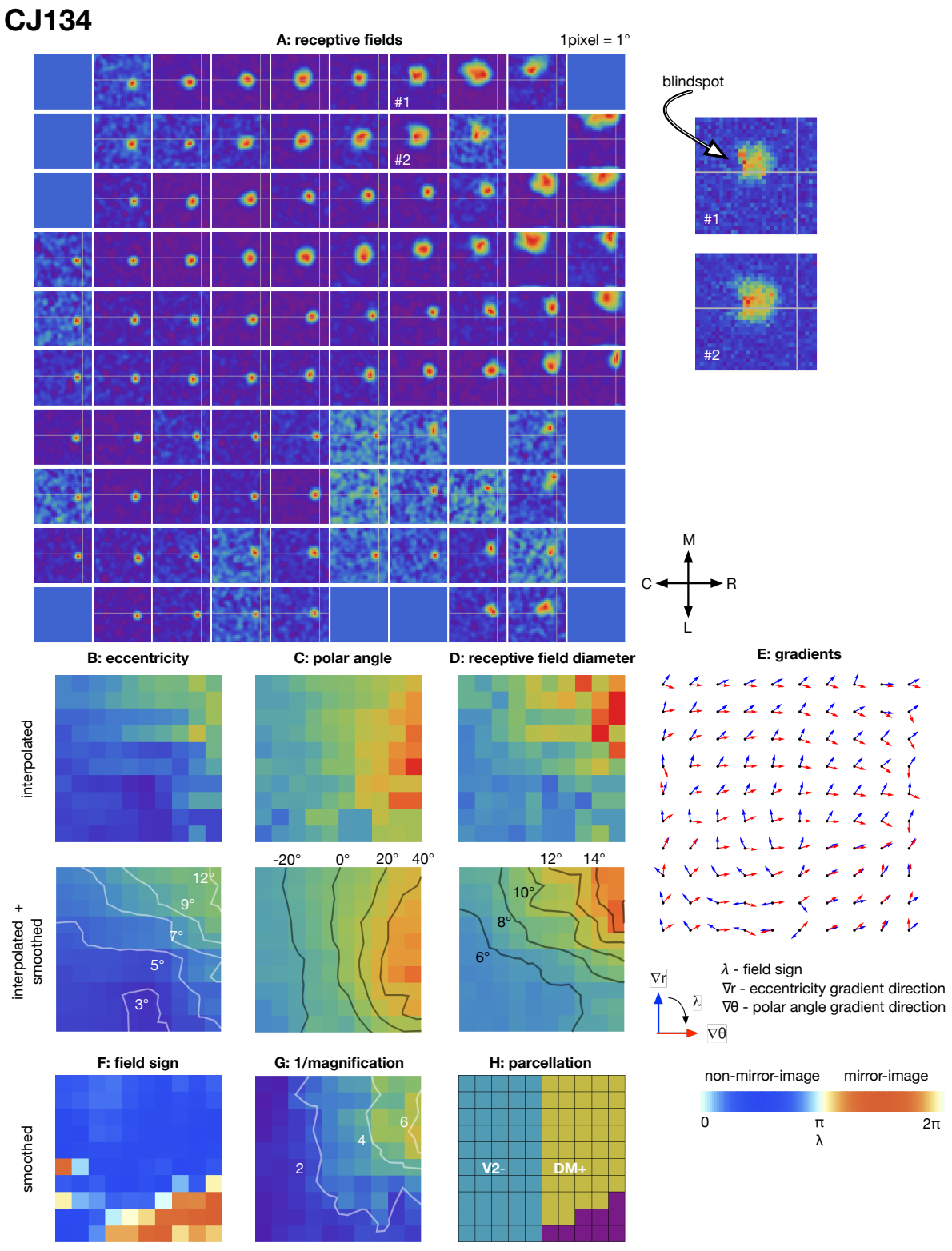

Supplementary Figure 1

Summary mapping data for case CJ134

(A) The outlines of the receptive fields for each channel, measured with a flashing square stimulus. In each plot of the receptive fields, the estimated horizontal and vertical meridians are indicated by thin white lines. For some cases, the representations of the blind spot were visible in some of the receptive field maps. Representative receptive field maps with “holes” (the blind spot) are shown on the right

without spatial smoothing. The correspondence between those maps and the plots for the entire array is indicated by numbers in white**. (B, C, D)** Maps of the eccentricity, polar angle, and diameter of the receptive fields without (top) and with (bottom) spatial smoothing**. (E)** The gradient vector fields used to estimate the field sign. The blue vectors represent the directions of the eccentricity gradient (∇r), and the red vectors represent the directions of the polar angle gradient ($\nabla \theta$). Field sign (λ) is the clockwise angle between the two vectors. **(F)** The map of field signs, illustrated with the color scale shown in the right**. (G)** The map of the reciprocals of the linear cortical magnification factor (unit: $^{\circ}/mm$). **(H)** The assignments of the electrode array channels to one of four areas (V2-, DM+, DM-, and others).

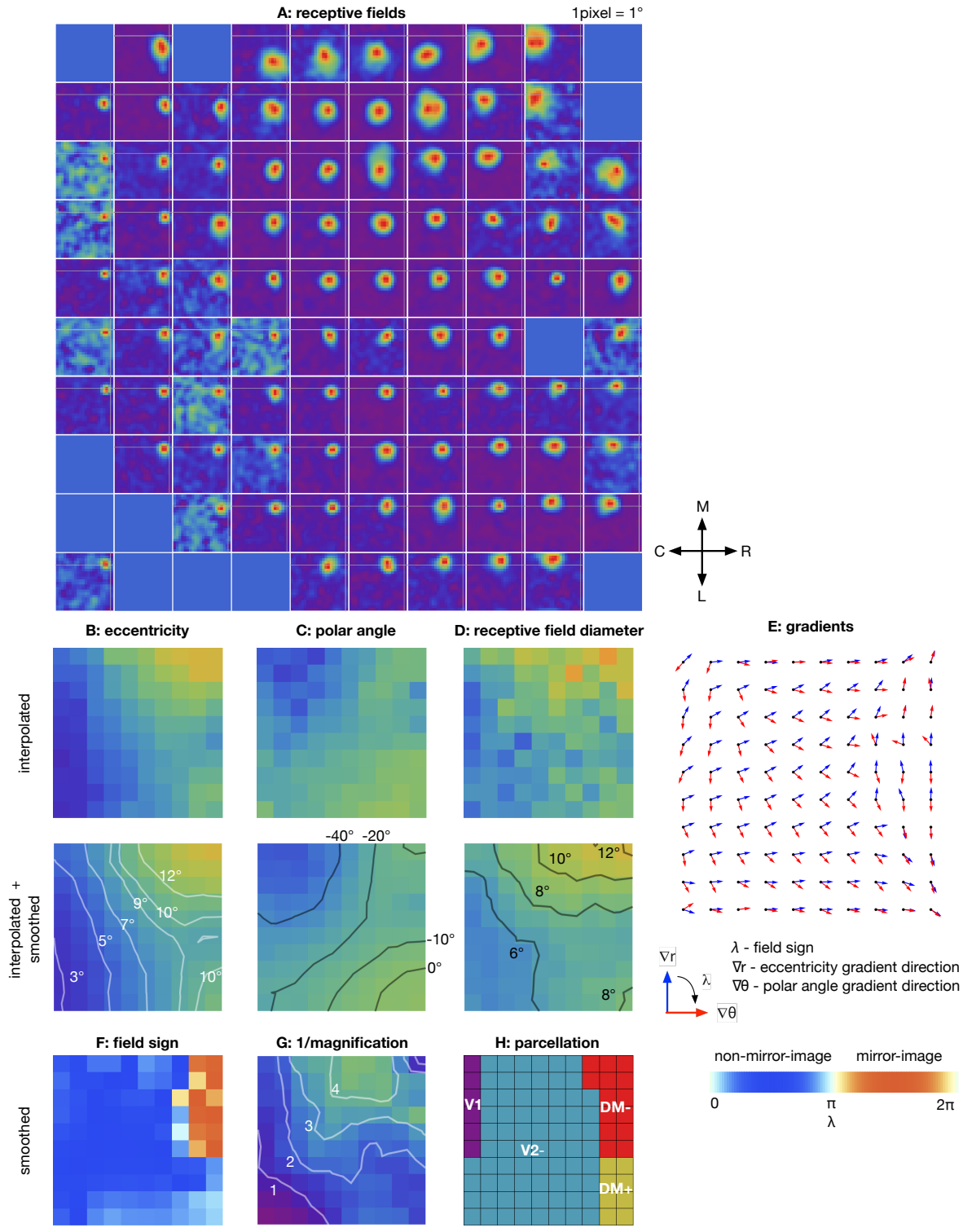

Supplementary Figure 2

Summary mapping data for case CJ139LH

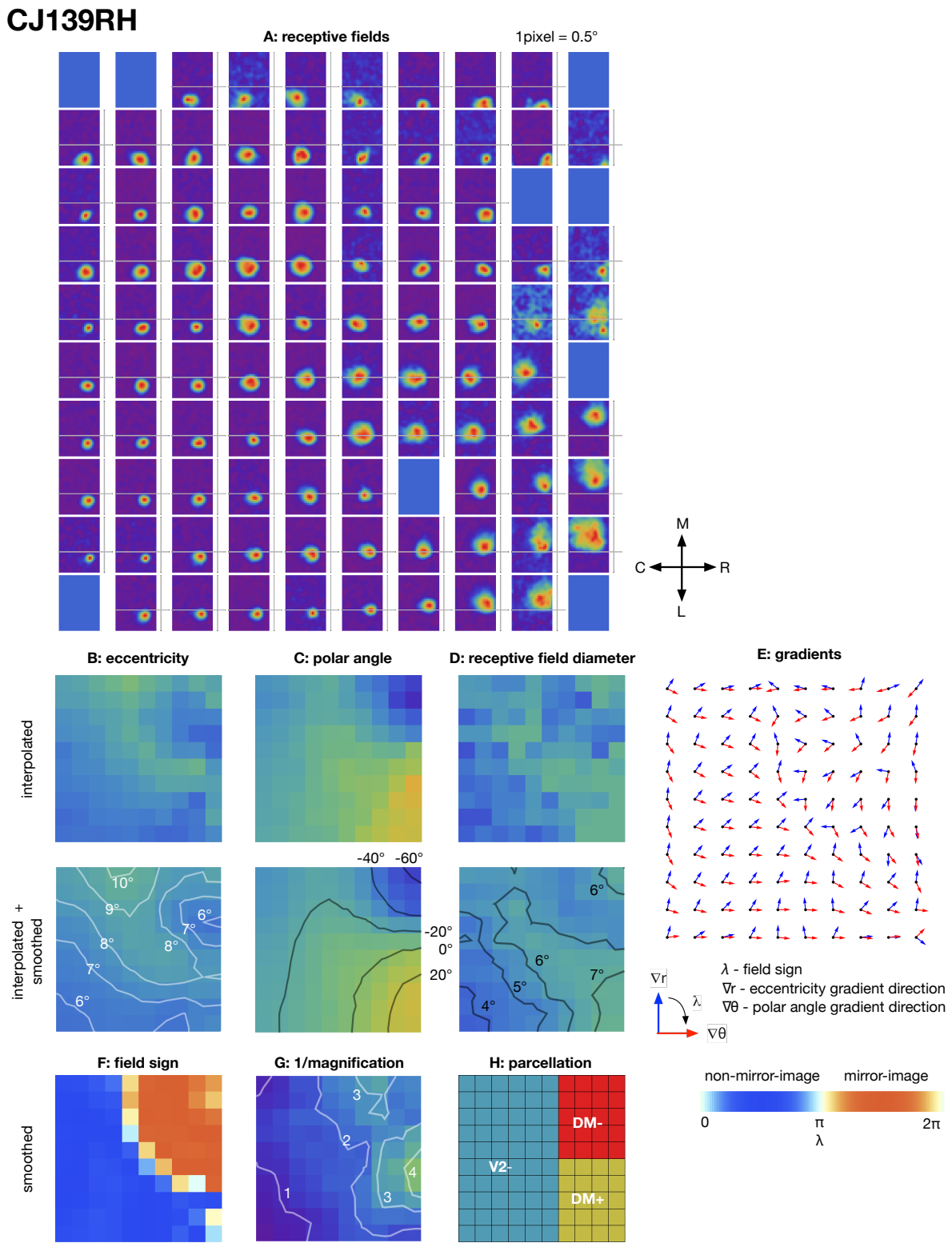

Supplementary Figure 3

Summary mapping data for case CJ139RH

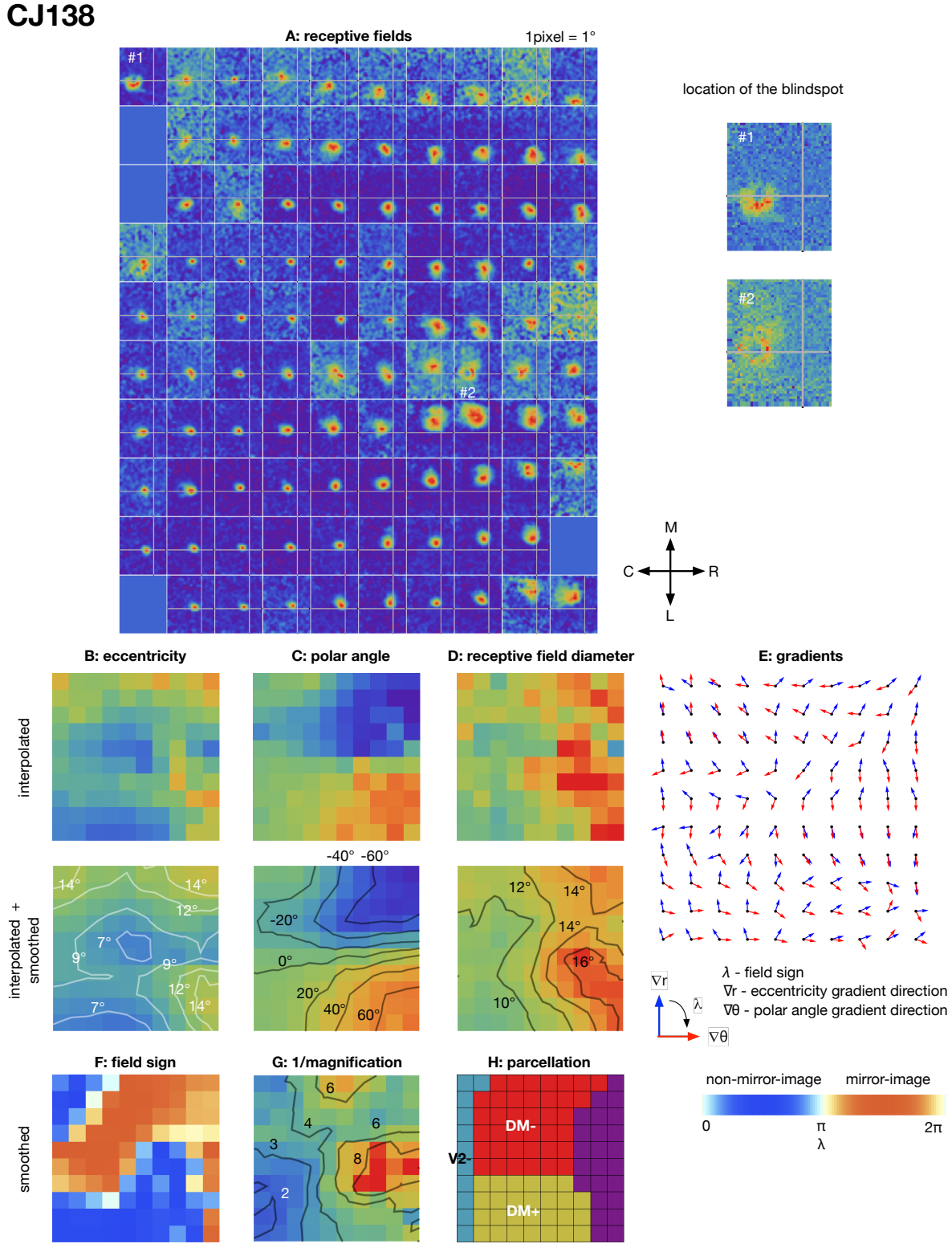

Supplementary Figure 4

Summary mapping data for case CJ138

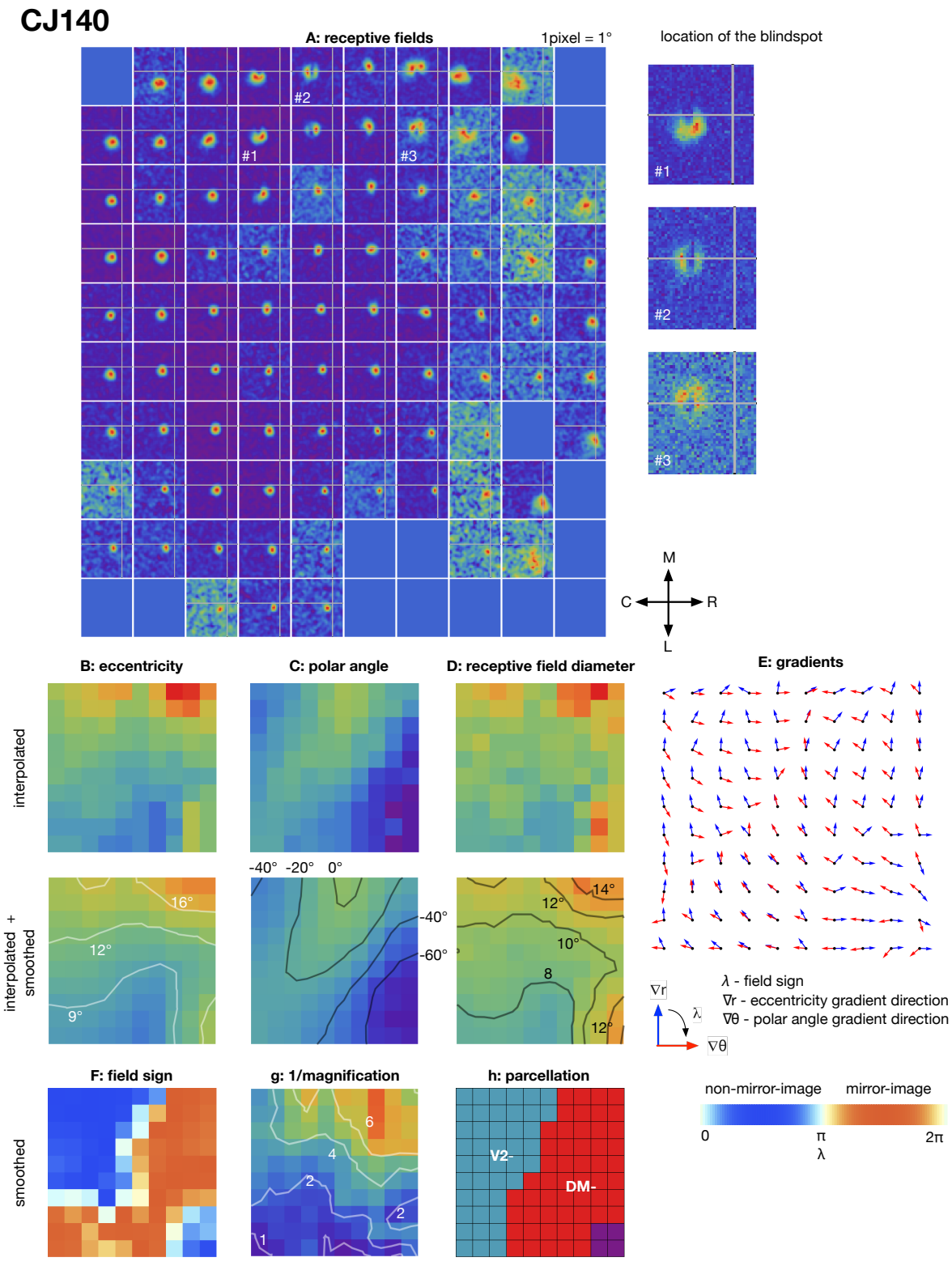

Supplementary Figure 5

Summary mapping data for case CJ140

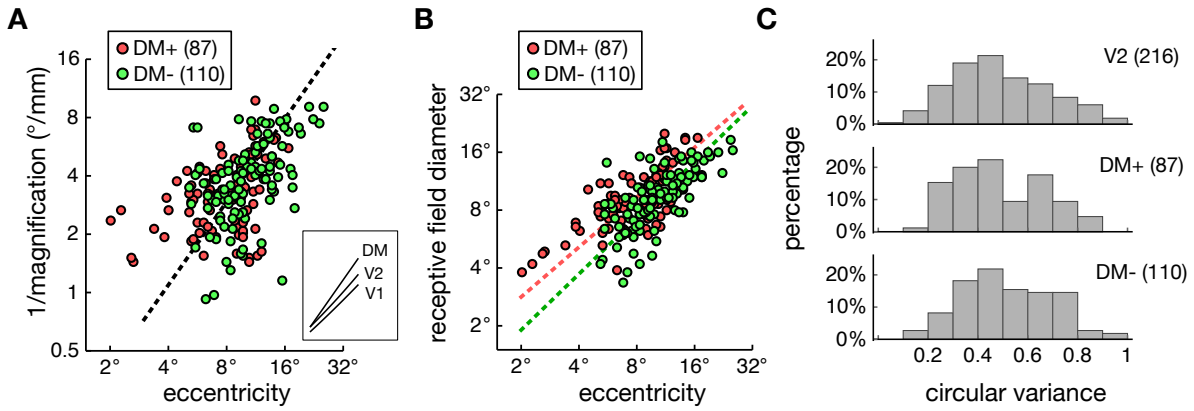

Supplementary Figure 6

Comparing the response characteristics of DM+ and DM- neurons

(A) The distributions of 1/M for DM+ and DM-, where M is the linear cortical magnification factor. The dashed regression line was calculated with data pooled from DM+ and DM-. Inset: The cortical magnification factor of DM compared to the marmoset V1 (Chaplin et al., 2013) and V2 (Rosa et al., 1997), in the eccentricity range of 5° to 20°.

(B) The distributions of receptive field diameters estimated for DM+ and DM-, as functions of the eccentricity. The dashed regression lines were calculated separately for DM+ (red) and DM- (green).

(**C**) The distributions of circular variance (a measure of orientation selectivity) for V2, DM+, and DM-. Most of neurons in DM+ and DM- are orientation tuned, in a distribution similar to that of V2.

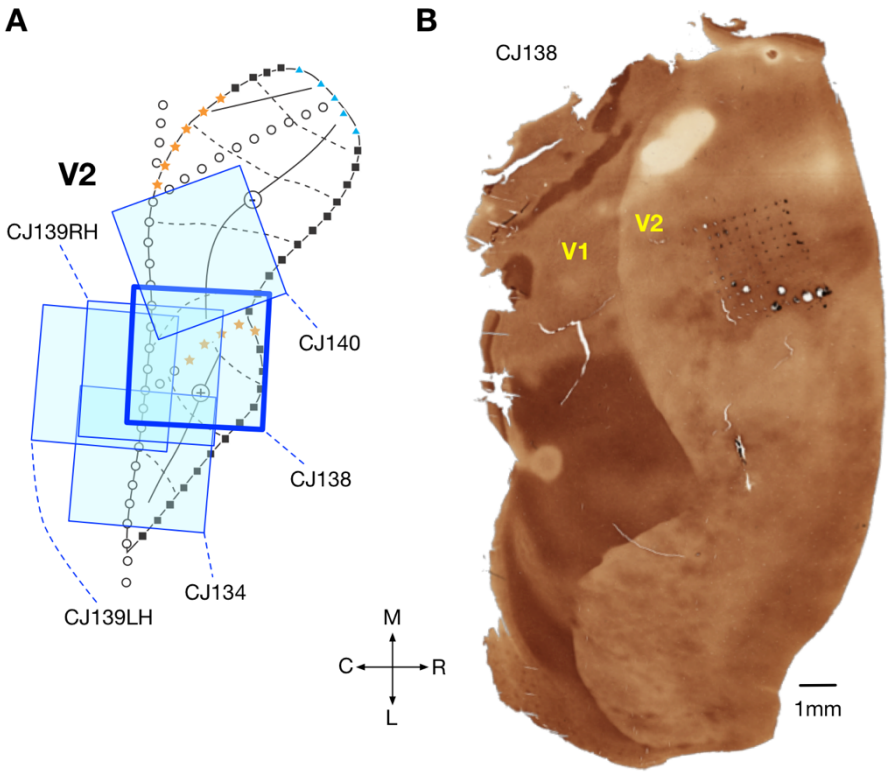

Supplementary Figure 7

Locations of the implanted arrays
(A) The relative locations of the implanted arrays, inferred from histology. **(B)** The flat-mounted occipital lobe (stained for cytochrome oxidase) of case CJ138. The marks left by the individual electrodes confirmed that the array was implanted immediately rostral to area V2. Abbreviations: M – medial; R – rostral; L – lateral; C – caudal.